Clusterin in Alzheimer's Disease: An Amyloidogenic Inhibitor of Amyloid Formation

Panagiotis M. Spatharas
National and Kapodistrian University of Athens
Georgia I. Nasi
National and Kapodistrian University of Athens
Paraskevi L. Tsiolaki
National and Kapodistrian University of Athens
Marilena K. Theodoropoulou
National and Kapodistrian University of Athens
Nikos C. Papandreou
National and Kapodistrian University of Athens
Andreas Hoenger
University of Colorado at Boulder
Ioannis P. Trougakos
National and Kapodistrian University of Athens
Vassiliki A. Iconomidou (veconom@biol.uoa.gr)
National and Kapodistrian University of Athens https://orcid.org/0000-0002-9472-5146

Research

Keywords: Clusterin, Molecular chaperones, Aggregation-prone regions, Amyloid, Amyloid-β, Amyloid inhibitors, Alzheimer's disease

Posted Date: June 16th, 2021

DOI: https://doi.org/10.21203/rs.3.rs-604024/v1

Version of Record: A version of this preprint was published at Biochimica et Biophysica Acta (BBA) - Molecular Basis of Disease on March 1st, 2022. See the published version at https://doi.org/10.1016/j.bbadis.2022.166384.

Clusterin in Alzheimer's disease: an amyloidogenic inhibitor of amyloid formation

Panagiotis M. Spatharas[1], Georgia I. Nasi[1], Paraskevi L. Tsiolaki[1, †], Marilena K. Theodoropoulou[1], Nikos C. Papandreou[1], Andreas Hoenger[2], Ioannis P. Trougakos[1], Vassiliki A. Iconomidou[1, *]

[1] Section of Cell Biology and Biophysics, Department of Biology, School of Sciences, National and Kapodistrian University of Athens, Panepistimiopolis, Athens 157 01, Greece

[2] University of Colorado at Boulder, Department of Molecular, Cellular and Developmental Biology, Boulder, CO 80309-0347, USA

[†] Present Address: Department of Biochemistry and Biophysics, University of California, San Francisco, California 94143-2240, USA

[*] Corresponding author: veconom@biol.uoa.gr

e-mails:

Panagiotis M. Spatharas: panspatharas@biol.uoa.gr

Georgia I. Nasi: gnasi@biol.uoa.gr

Paraskevi L. Tsiolaki: etsiolaki@biol.uoa.gr

Marilena K. Theodoropoulou: mtheod@biol.uoa.gr

Nikos C. Papandreou: npapand@biol.uoa.gr

Andreas Hoenger: Andreas.Hoenger@Colorado.edu

Ioannis P. Trougakos: itrougakos@biol.uoa.gr

Vassiliki A. Iconomidou: veconom@biol.uoa.gr

Abstract

Background: Clusterin is a heterodimeric glycoprotein (α- and β-chain), which has been described as an extracellular molecular chaperone. In humans, clusterin is an amyloid associated protein, co-localizing with fibrillar deposits in Alzheimer's disease. To clarify its implication in the disease, we provide evidence that clusterin has intrinsic amyloidogenic properties, which are intertwined with its inhibitory effect on amyloid-β fibril formation.

Methods: Aggregation-prone regions of human clusterin were predicted by AMYLPRED. Synthetic peptide-analogues of each region underwent *in vitro* aggregation assays, namely, examination with transmission electron microscopy, X-Ray diffraction from oriented fibers, ATR FT-IR spectroscopy, and Congo Red birefringence assays. The same peptide-analogues were co-incubated with amyloid-β and their potential as inhibitors was tested with thioflavin T fluorescence emission measurements and transmission electron microscopy. Molecular dynamics simulations were performed to gain insight into the interaction between amyloid-β and the peptide-analogues.

Results: Clusterin peptide-analogues form amyloid-like fibrils, as revealed by transmission electron microscopy. They can form fibers that give cross-β X-ray diffraction patterns and ATR FT-IR spectroscopy confirms the dominance of β-strand secondary structure. They also exhibit apple-green birefringence, when stained with Congo Red and examined between crossed polars of a polarizing light microscope. Furthermore, when amyloid-β is co-incubated with clusterin's peptide analogues, it shows decreased thioflavin T fluorescence emission over time, while the formation of amyloid-β amyloid fibrils is diminished, as confirmed by transmission electron microscopy. The inhibitory effect of clusterin-peptide analogues on amyloid-β fibril formation was ascertained though molecular dynamics simulations.

Conclusions: Clusterin has multiple aggregation-prone regions in its α-chain and these regions have a functional role in the inhibition of amyloid-β fibril formation.

Keywords

Clusterin, Molecular chaperones, Aggregation-prone regions, Amyloid, Amyloid-*β*, Amyloid inhibitors, Alzheimer's disease

Background

Since the 17th century, physicians had already started to describe clinical disorders that were later included in a broad group of diseases, nowadays known as amyloidoses [1]. Prime examples are Alzheimer's disease (AD), Parkinson's disease, type 2 diabetes, and AL amyloidosis [2]. It is widely considered that these diseases are closely associated with the accumulation and close packing of normally soluble proteins, which end up creating highly ordered, insoluble aggregates. The so-called amyloid fibrils, are deposited extracellularly in organs or tissues, causing significant damage [2].

Molecular chaperones can inhibit amyloid formation in its early stages, thus preventing amyloid-related cytotoxicity [3]. Recent studies, though, have shown that molecular chaperones can have amyloidogenic properties [4-7], despite their seemingly contradicting physiological function. *In vitro* experiments performed by our team have hinted that clusterin could be such a protein [7]. Clusterin is a ubiquitous, conserved mammalian glycoprotein, whose main isoform is secreted and has been described as an extracellular molecular chaperone [8]. Human clusterin precursor is a 449 residue-long polypeptide chain, which, after having its signal peptide removed, is reduced to 427 residues, and goes through several post-translational modifications [8]. Mature clusterin is cleaved in two chains —α-chain, consisting of 222 residues and β-chain, consisting of 205 residues— with five disulfide bonds forming between them [8]. Its molecular weight is approximately 80 kDa, almost 30% of it being carbohydrates, added by glycosylation [8]. Clusterin's structure has yet to be experimentally determined, but is believed to contain three long molten globule-like regions and five amphipathic α-helices, which allow for hydrophobic interactions with its client-proteins [9].

Under normal circumstances, clusterin exists in solution as heterogeneous aggregates [10]. It has been suggested that, at mildly acidic pH [10], these aggregates disassociate and the disassociated chaperone-active subunits function in an ATP-independent manner [11]. They

bind misfolded client-proteins and form a high molecular weight complex. The formation of the complex allows for stabilization of the misfolded proteins, which are consequently refolded by other molecular chaperones [9] (visualized in Fig 1). Clusterin's ever-growing list of known clients includes a variety of proteins, such as cellular receptors, apolipoproteins, the complement complex, immunoglobulins, amyloid-forming proteins, and non-protein molecules, like lipids and heparin [12].

Figure 1. Representation of clusterin's molecular chaperone activity. (1) Under stress (low pH), native proteins (NP) may partially unfold and become misfolded. (2) At slightly acidic pH, clusterin's (CLU) oligomers start disassociating and the chaperone-active clusterin subunits get released. (3) The free clusterin subunits bind the misfolded proteins (MP) and form a complex, effectively stabilizing them, (4) while other molecular chaperones refold them to their native state. (5) If this mechanism proves ineffective, the misfolded proteins may form aggregates.

Having such a broad range of clients, it is only logical that clusterin contributes to many physiological and pathological processes [13]. AD is one of the most notable pathologies in which clusterin is involved [12]. Consistent with its chaperone function, clusterin keeps the amyloid-β (Aβ) peptide soluble while transporting it in biological fluids, modulates its permeation through the blood-brain barrier and contributes to its clearance, effectively halting amyloid formation [14]. In direct contradiction to that, it has been reported that clusterin contributes to the early stages of AD pathogenesis [15,16]. To this day, clusterin's role in AD is yet to be fully understood. Despite the mystery surrounding clusterin's implication in AD, it is a known fact that it co-localizes with Aβ fibrillar deposits [12]. This is also true for other amyloidoses, in which clusterin is an amyloid-associated protein [17].

It can be assumed that clusterin is found in the amyloid deposits because it is drifted along by its client-proteins. In this study, we examined a different scenario, one that doesn't rule out the possibility of clusterin being amyloidogenic itself. We used AMYLPRED [18], a consensus algorithm for the prediction of amyloid propensity, in order to identify aggregation-prone

regions in clusterin α-chain. We had peptide-analogues of each region chemically synthesized and experimentally demonstrated that all of them can form amyloid-like fibrils *in vitro*. The same peptide-analogues, despite being amyloidogenic, can inhibit Aβ fibril formation. Based on our findings, we proposed a putative mechanism in which clusterin prevents amyloid formation. The suggested mechanism could also explain the contradictory reports that hint at clusterin's implication in the acceleration of the appearance of AD symptoms. At the same time, we hope that the basis of clusterin's amyloid inhibiting activity could give insight into the implementation of peptide-based amyloidogenesis inhibitors in the treatment of amyloidoses.

Methods

Prediction of potential aggregation-prone and natively disordered regions in human clusterin

AMYLPRED [18], a consensus algorithm for the prediction of amyloid propensity, was used for the identification of aggregation-prone regions in wild-type, mature clusterin (Uniprot AC: P10909). The α-chain, which is our focus in the current study, has five such regions. The first one (^{12}NFHAMFQ^{18}) has previously been studied by our lab and proved to exhibit amyloidogenic properties *in vitro* [7]. This time, we opted to study the remaining four, those being ^{31}MDIHF^{35}, ^{82}LSV^{84}, ^{155}YYLRVTT^{161}, and ^{177}EVVVKLF^{183}. Natively disordered regions were predicted using PONDR® VLTX (http://www.pondr.com).

Peptide synthesis

All peptide-analogues were synthesized and lyophilized by GeneCust Europe, France. The exact sequences for the peptide-analogues were NFHAMFQ, AMDIHF, ILSVD, NLSVD, YYLRVTT, and EVVVKLF. The regions that were used for the second and third peptide-analogues were ^{30}AMDIHF^{35} and ^{81}ILSVD^{85}, which are extensions of the originally predicted regions. NLSVD is a mutant counterpart of ILSVD. The purity of all the synthesized peptides was higher than 98%, with the N- and C-terminals being free.

125 Aβ_{42} was also synthesized and lyophilized by GeneCust Europe, France. The exact sequence is
126 DAEFRHDSGYEVHHQKLVFFAEDVGSNKGAIIGLMVGGVVIA. The purity of the peptide was higher
127 than 95%, with the N- and C-terminals being free.

128 **Sample preparation**

129 **Disaggregation of pre-existing aggregates:** Each lyophilized peptide was dissolved in
130 1,1,1,3,3,3-Hexafluoro-2-propanol (HFIP; Sigma-Aldrich) at a concentration of 1 mg/mL. All
131 clusterin peptides were mixed with equimolar amounts of Aβ_{42}. Individual peptide solutions and
132 Aβ_{42}-clusterin peptide solutions were left to dry overnight in a fume hood, at room temperature,
133 until thin peptide-containing films were created. The peptide-containing films were stored at -
134 20 °C.

135 ***In vitro*** **fibril formation:** The peptide-containing films were left at room temperature for 30
136 minutes and dissolved in 0.1 M HEPES buffer (pH=7.4; Biosera) or dH_2O (pH=5.57), at
137 concentrations ranging from 10 µM to 1 mM. The peptide solutions were incubated for 1 week
138 at 37 °C unless stated otherwise.

139 **Transmission Electron Microscopy (TEM).**

140 A 3 µL droplet of 100 or 500 µM peptide solution was applied to glow-discharged 400-mesh
141 carbon-coated copper grids for 60 seconds. Directly afterwards, the grids were stained with a 3
142 µL droplet of 2% (w/v) aqueous uranyl acetate for another 60 seconds. Excess stain was blotted
143 away with filter paper and air-dried. The grids were examined with a Morgagni 268
144 transmission electron microscope, operated at 80 kV. Digital acquisitions were performed with
145 an 11 Mpixel side-mounted Morada CCD camera (Soft Imaging System, Muenster, Germany).

146 **X-ray diffraction from oriented protein fibers.**

147 **Oriented fiber formation:** 1 mM peptide solutions were incubated for two weeks, to form
148 viscous solutions, which facilitate the formation of oriented fibers. A 10 µL droplet of each
149 peptide solution was placed between two quartz capillaries covered with wax, spaced

approximately 1.5 mm apart, and mounted horizontally on a glass substrate, as collinearly as possible. The droplet was allowed to dry for 3 days until oriented fibers were formed.

X-ray diffraction and analysis: The oriented fibers were shot with X-rays and diffracted. The X-ray diffraction pattern was collected using a SuperNova-Agilent Technologies X-ray generator, equipped with a 135 mm ATLAS CCD detector and a 4-circle kappa goniometer, at the Institute of Biology, Medicinal Chemistry and Biotechnology, National Hellenic Research Foundation (CuKα high intensity X-ray micro-focus source, λ = 1.5418 Å), operated at 50 kV, 0.8 mA. The specimen-to-film distance was set at 52mm and the exposure time was set to 200s. The X-ray patterns were initially viewed using CrysAlisPro [19] and afterwards measured with iMosFLM [20].

Attenuated total reflectance Fourier-transform infrared (ATR FT-IR) spectroscopy.

A 10 μL droplet of 500 μM peptide solution was cast on a front-coated Au mirror and left to dry slowly at room temperature until a thin peptide-containing film was created. Infrared spectra were obtained from these films at a resolution of 4 cm^{-1}, utilizing an IR microscope (IRScope II by Bruker Optics) equipped with a Ge attenuated total reflectance (ATR) objective lens (20x) and attached to a Fourier-transform infrared (FT-IR) spectrometer (Equinox 55, by Bruker Optics). Ten 32-scan spectra were collected from each sample and averaged to improve the sound/noise (S/N) ratio. Both are shown in the absorption mode after correction for the wavelength dependence of the penetration depth (pd-λ). Absorption band maxima were determined from the minima in the second derivative of the corresponding spectra. Derivatives were computed analytically using routines of the Bruker OPUS/OS2 software, including smoothing over a ±13 cm^{-1} range around each data point, performed by the Savitzky–Golay [21] algorithm. Data were visualized using OriginPro 7 (OriginLab Corporation).

Congo Red Birefringence Assay.

A 3 μL droplet of the 500 μM peptide solution was applied to glass slides and stained with a 10 mM Congo Red (Sigma-Aldrich) solution in PBS (137 mM NaCl, 27 mM KCl, 100 mM Na_2HPO_4, 18 mM KH_2PO_4, pH=7.4) or dH_2O for approximately 30 minutes. Then, they were washed several times with 90% ethanol and were left to dry approximately for 10 minutes. The samples were observed under bright field illumination and between crossed polars, using a Leica MZ7.5 polarizing stereomicroscope, equipped with a Sony α6000 camera.

Thioflavin T (ThT) Kinetic Assay

ThT fluorescence measurements were conducted at 37 °C, in black 96-well plates with flat, clear bottoms, using a Tecan Spark microplate reader. The top of the plates was sealed with microplate covers and the fluorescence readings were performed through the bottom. A 444 nm filter was used for excitation and a 484 nm filter for emission. HFIP peptide films were dissolved in DMSO (Applichem GmbH) and diluted in HEPES for a final DMSO concentration of less than 5% v/v. The reaction solutions contained freshly prepared 10 μM disaggregated peptide solutions (individual Aβ_{42} or Aβ_{42}-clusterin peptide solutions) and 25 μM ThT (Sigma-Aldrich) in dH_2O. ThT background fluorescence was measured in the absence of peptide solutions. Each experiment was conducted in triplicates. Measurement lasted for 50 hours and fluorescence readings were collected every 15 minutes. ThT background fluorescence was subtracted from the peptide fluorescence readings at each time point. Standard deviation was calculated, and the data was normalized. 100 arbitrary units correspond to maximum individual Aβ_{42} fluorescence intensity. Data were visualized using RStudio (package ggplot2).

Molecular Dynamics Simulations

Structure acquisition and molecular docking. Simulations were performed using an NMR structure of pentameric Aβ_{42} (PDB ID: 2BEG) [22], while a structure for EVVVKLF was generated through the "Builder" tool in PyMOL [23]. Aβ_{42}-EVVVKLF docking was performed through the

automated protein docking server ClusPro [24-27]. The generated clusters were evaluated with the balanced scoring scheme.

Molecular dynamics simulations. The derived complex was subjected to molecular dynamics simulations via GROMACS v. 2018.1 [28]. The simulations employed the AMBER99SB-ILDN protein, nucleic AMBER94 force-field [29]. The complex was placed in a 1.2 nm cubic box of 3-point model (TIP3P) water [30] and the system was ionized using NaCl molecules, mimicking neutral pH conditions. Each simulation system was subjected to energy minimization, in a maximum of 2000 steps, using the steepest descent algorithm, followed by two stages of equilibration simulations with position restraints applied on protein coordinates. Specifically, a 100 ps simulation was performed in the canonical (NVT) ensemble to equilibrate temperature at 310 K, using the Berendsen-thermostat [31]. Following the first equilibration, a 100 ps simulation was performed in the isothermal-isobaric (NPT) ensemble to control pressure isotopically at 1.013 bar (1 atm), using the Berendsen weak coupling algorithm [32] and the Berendsen-thermostat at 310 K. Finally, the MD simulation with position restraints removed was carried out for 600ns at 310K. One control run of individual $A\beta_{42}$ was also performed. Periodic boundary conditions were applied to all directions. The LINCS algorithm [33] was applied to model bond constraints, enabling the use of a 2 fs time-step. Short-range non-bonded interactions were modeled using a twin-range cutoff at 0.8 nm, while long-range electrostatic interactions were modeled using the Particle Mesh Ewald (PME) method, with a Fourier grid spacing at 0.12 nm [34].

Analysis of simulation results. Simulation results were analyzed using various GROMACS utilities, and Visual Molecular Dynamics (VMD) v. 1.9.4 [35]. Structural stability was checked using the “rms” tool [36]. Secondary structure was calculated using the “do_dssp” tool [37,38]. Hydrogen bonds were calculated using the “hbond” tool [39]. Frames were extracted every 100ps and used for the analysis. Pictures were collected with UCSF Chimera [40] or PyMOL [23].

Results

All wild-type clusterin α-chain peptide-analogues form amyloid-like fibrils *in vitro*

According to the prediction of AMYLPRED, clusterin α-chain has five aggregation-prone regions. The peptide-analogues that correspond to those regions are NFHAMFQ, AMDIHF, ILSVD, YYLRVTT, and EVVVKLF, as depicted in Fig 2. NFHAMFQ has previously been studied by our lab and proved to exhibit amyloidogenic properties *in vitro* [7]. Our current findings reveal that AMDIHF, ILSVD, YYLRVTT, and EVVVKLF can also be characterized as amyloidogenic *in vitro*, making a total of five experimentally verified aggregation-prone regions in clusterin α-chain. Characterization was based on the tinctorial criteria, which are commonly used for the identification of amyloid fibrils (transmission electron microscopy, X-ray diffraction from protein fibers, ATR FT-IR spectroscopy, and Congo Red birefringence assay) [41].

Figure 2. A simple representation of clusterin's two chains. Each chain is colored grey, with a black outline, and its sequence is numbered as found in the mature protein. The α-chain consists of 222 amino acid residues. The β-chain is slightly shorter, consisting of 205 amino acid residues. The two chains are joined by five disulfide bonds, depicted as black dots. The aggregation-prone regions of the α-chain are depicted as black rectangles on clusterin's sequence.

Transmission electron micrographs show that AMDIHF, ILSVD, YYLRVTT, and EVVVKLF self-assemble into amyloid-like fibrils (Fig 3 A-D, respectively). AMDIHF fibrils exhibit considerable polymorphism, forming both supercoils and tapes (Fig S1 A-C), while EVVVKLF fibrils form large twisting ribbons, with a 162 nm pitch (Fig S1D). ILSVD forms amyloid-like fibrils that are packed more densely in comparison to the other peptides (Fig 3), indicating that it could be the most aggregation-prone region in clusterin α-chain.

Figure 3. All the peptide-analogues fulfill the experimental criteria. (A-D) Transmission electron micrographs of amyloid-like fibrils derived from 500 μm solutions of peptides AMDIHF, ILSVD, YYLRVTT, and EVVVKLF, respectively. White arrows mark single fibrils with the diameter of typical amyloid fibrils. (E-H) X-ray diffraction patterns of oriented fibers, derived from 1 mM solutions of the four peptides,

respectively. Reflections marked with arrows are indicative of the "cross-*β*" structure, which amyloids typically have. (I-L) Photomicrographs of gels, derived from 500 μM solutions of the four peptides, respectively. Congo red is bound, as seen under bright field illumination (upper). The apple-green birefringence that amyloids typically exhibit is observed under crossed polars (lower). (M-P) ATR FT-IR spectra (1100–1800 cm^{-1}) produced from thin hydrated films created by 500 μM solutions of the four peptides, respectively. Fibrils derived from each peptide have a *β*-sheet secondary structure, as hinted by the presence of strong amide I and II bands.

Figure S1. Electron micrographs of polymorphic structures formed by AMDIHF and EVVVKLF amyloid-like fibrils. Samples were incubated for 7 days, at 37 °C and 500 μM. (A) Supercoil formed by AMDIHF amyloid-like fibrils. (B) Tape formed by laterally interacting AMDIHF amyloid-like fibrils. (C) An amyloid-like fibril formed by AMDIHF, with a diameter of approximately 160 Å, is split into two 80 Å fibrils. (D) EVVVKLF amyloid-like fibrils form large, twisting ribbons, with a 162 nm pitch, a minimum width of 35 nm, and a maximum width of 53 nm.

Oriented fibers formed by each peptide solution, produce X-ray diffraction patterns, indicative of the presence of the "cross-*β*" structure. Most reflections are ring-like, most likely because the fibrils are not perfectly aligned in a parallel manner [42]. The exact measurements for each of the four diffraction patterns can be seen in Fig 3 (E-H). It is worth pointing out that the EVVVKLF diffraction pattern has two equatorial reflections, one at 8.12 and one at 12.12 Å. Upon closer examination of the twisting ribbons, formed by EVVVKLF (Fig S1D), the maximum width is observed in the middle of the pitch, and measures approximately 53 nm, while the minimum width is observed at the site of the twist, and measures approximately 35 nm. The quotient of the two equatorial reflections (8.12 :12.12 ≈0.67) is roughly equal to the quotient of the minimum and maximum ribbon width (35 : 53 ≈ 0.66). The equatorial reflections are indicative of the distance between packed *β*-sheets. Thus, EVVVKLF fibrillar structures are probably formed by β-sheets that are more tightly packed at the twist, in comparison to the middle of the ribbon. The periodicity of the tightening and untightening of the β-sheets is revealed by a combination of X-ray and TEM data.

The dominance of the *β*-sheet secondary structure is supported by ATR FT-IR spectroscopy data, since the spectra of all four peptide-analogues reveal bands that can be assigned to *β*-sheets [43] (Table 1 and Fig 3 M-O).

Table 1. Bands observed in the ATR FT-IR spectra obtained from thin hydrated films produced by AMDIHF, EVVVKLF, YYLRVTT, and ILSVD solutions, respectively, and their tentative assignments.

AMDIHF bands	ILSVD bands	YYLRVTT bands	EVVVKLF bands	Band assignments
1134	1140	1138	1138	TFA
1186	1186	1188	1182	TFA
1201	1202	1200	1202	TFA
-	-	1516	-	Tyrosine
1543	1537	1537	1537	*β*-sheet
1631	1624	1624	1626	*β*-sheet
1668	1668	1666	1676	TFA
-	1692	1693	1690	Antiparallel *β*-sheet

Every peptide binds Congo Red, as seen under bright field illumination in a polarizing stereomicroscope (Fig 3 I-L, upper). When the polars are crossed, the peptides exhibit the apple-green birefringence (Fig 3 I-L, lower) that amyloids typically exhibit.

NLSVD, a mutant counterpart of ILSVD, does not exhibit amyloidogenic properties

Recent studies have identified a novel pathological mutation on clusterin's gene, in AD patients. In particular, p.I360N changes the aggregation-prone region ^{81}ILSVD^{85} to ^{81}NLSVD^{85} [44]. The resulting sequence is not predicted by AMYLPRED, hinting that it is not aggregation-prone. To experimentally confirm that the mutated region is not aggregation-prone, we had NLSVD chemically synthesized. Indeed, transmission electron microscopy (TEM) shows that NLSVD does not self-assemble into amyloid fibrils (Fig S2A). Also, NLSVD does not form oriented fibers, suitable for X-ray diffraction, hinting that there are no fibrils in its solution. Finally, when

stained with Congo Red and stereoscopically observed between crossed polars, it does not exhibit apple-green birefringence (Fig S2B).

Figure S2. The mutant NLSVD does not form amyloid-like fibrils and does not inhibit Aβ_{42} fibril formation. (A) Electron micrographs reveal that NLSVD 500 μM solution does not contain amyloid-like fibrils, after 7 days of incubation. (B) Photomicrographs of gels derived from NLSVD 500 μM solution. Congo red is faintly bound, as seen under bright field illumination (upper) and apple-green birefringence is not exhibited under crossed polars (lower). (C) Electron micrographs of Aβ_{42}+NLSVD (100 μM Aβ_{42} and 100 μM NLSVD) reveal that NLSVD does not inhibit amyloid fibril formation, after 7 days of incubation. Aβ_{42} fibrils (white arrow) are wider than those of individually incubated Aβ_{42} fibrils (Figure 4d) and have a higher tendency to interact laterally and form loosely bound tapes (blue arrows).

Clusterin *α*-chain peptide-analogues inhibit Aβ_{42} amyloid formation *in vitro*

Full-length clusterin is known to inhibit Aβ fibril formation *in vitro* [45]. We aimed to pinpoint segments of its sequence that could act as catalysts of said inhibition. Each clusterin peptide-analogue was co-incubated with equimolar amounts of Aβ_{42} and the aggregation kinetics were evaluated with Thioflavin T (ThT) fluorescence measurements over time and TEM.

ThT fluorescent measurements reveal that individual Aβ_{42} starts forming fibrils almost immediately and reaches maximal fluorescence signal after approximately 7 hours. When co-incubated with clusterin peptide-analogues (Aβ_{42}+NFHAMFQ, Aβ_{42}+AMDIHF, Aβ_{42}+ILSVD, Aβ_{42}+YYLRVTT, and Aβ_{42}+EVVVKLF), Aβ_{42} exhibits decreased emission. ILSVD and especially EVVVKLF seem to be the most potent inhibitors (Fig 4J and 4P, respectively). As previously shown, individual ILSVD is incredibly amyloidogenic, as is Aβ_{42}. The fact that interaction between the two leads to decreased fibril formation, hints that peptides with high amyloidogenic potential, could negate each other's fibril-forming properties. EVVVKLF bears some sequence similarity with ^{16}KLVFFA^{21}, a key amyloid-forming segment of Aβ_{42} [46]. Considering that peptide-analogues derived from ^{16}KLVFFA^{21} have been suggested as potential therapeutic agents for the treatment of AD [47], it is not surprising that EVVVKLF has the highest

inhibiting effect among the five peptides. NFHAMFQ and AMDIHF also seem to inhibit Aβ_{42} fibril formation (Fig 4F and 4H, respectively), but their potential as inhibitors is less significant than that of ILSVD and EVVVKLF. YYLRVTT effectively delays fibril formation, but after approximately 20 hours, fluorescence signal begins to rise (Fig 4N). After 40 hours, Aβ_{42}+YYLRVTT reaches fluorescence intensity levels which are comparable to those of individual Aβ_{42}.

Figure 4. Clusterin peptide-analogues inhibit or delay Aβ_{42} fibril formation. (A-D) Transmission electron micrographs of Aβ_{42}, incubated for 0, 1, 3, and 7 days, respectively. Amyloid fibrils are observed from day 1 to day 7. The number of fibrils raises as incubation time increases. (E, F) Transmission electron micrograph and ThT fluorescence emission spectrum of Aβ_{42} co-incubated with NFHAMFQ for 7 days and over a period of 50 hours, respectively. (G, H) Transmission electron micrograph and ThT fluorescence emission spectrum of Aβ_{42} co-incubated with AMDIHF for 7 days and over a period of 50 hours, respectively. (I, J) Transmission electron micrograph and ThT fluorescence emission spectrum of Aβ_{42} co-incubated with ILSVD for 7 days and over a period of 50 hours, respectively. (K, L) Transmission electron micrograph and ThT fluorescence emission spectrum of Aβ_{42} co-incubated with the mutant peptide, NLSVD, for 7 days and over a period of 50 hours, respectively. (M, N) Transmission electron micrograph and ThT fluorescence emission spectrum of Aβ_{42} co-incubated with YYLRVTT for 7 days and over a period of 50 hours, respectively. (O, P) Transmission electron micrograph and ThT fluorescence emission spectrum of Aβ_{42} co-incubated with EVVVKLF for 7 days and over a period of 50 hours, respectively. Error bars in ThT fluorescence emission spectra represent standard deviation among triplicates. TEM experiments contained 100 µM Aβ_{42} and 100 µM clusterin peptide-analogues, while ThT experiments contained 10 µM and 10 µM, respectively.

TEM confirms that all five peptide-analogues inhibit or delay Aβ_{42} fibril formation, after 7 days of incubation. When individually incubated, Aβ_{42} forms straight and unbranched fibrils with indefinite length and a diameter of approximately 80 Å (Fig 4 B-D). A small number of fibrils is observed after 1 day of incubation (Fig 4B). The population of fibrils increases significantly after 3 days (Fig 4C) and reaches its maximum after 7 days (Fig 4D). As expected, ILSVD and EVVVKLF prove to be the most potent inhibitors (Fig 4I and 4O, respectively). The entire grids were

thoroughly examined, and no fibrils were observed. NFHAMFQ and AMDIHF also inhibit Aβ_{42} fibril formation, as fibrils were not observed anywhere on the grid (Fig 4E and 4G, respectively). However, both seem to induce the formation of amorphous aggregates. YYLRVTT seems to delay, but not inhibit fibril formation. In contrast to the other peptides, fibrils can be observed (Fig 4M). The number of fibrils is similar to that of individual Aβ_{42}, after 1 day of incubation. Much like NFHAMFQ and AMDIHF, YYLRVTT also seems to induce the formation of amorphous aggregates.

On the contrary, ThT kinetics and TEM show that NLSVD, the mutant counterpart of ILSVD, does not inhibit Aβ_{42} amyloid formation *in vitro*. Aβ_{42} and Aβ_{42}+NLSVD fluorescence curves mostly overlap, while Aβ_{42}+NLSVD show a slightly enhanced fluorescence peak (Fig 4K). Transmission electron micrographs reveal that Aβ_{42} fibril morphology is different from that of Aβ_{42}+NLSVD. Aβ_{42}+NLSVD fibrils, after 7 days of incubation, are more densely packed and slightly wider than those of individual Aβ_{42}, after the same incubation period (Fig 4L and Fig S2C, white arrow). Furthermore, Aβ_{42}+NLSVD fibrils tend to interact laterally and form loosely bound tapes (Fig S2C, blue arrows).

Computational insight into the inhibition of Aβ_{42} fibril formation by EVVVKLF

To shed light on the interaction between Aβ_{42} and EVVVKLF, the most potent of the five peptide-inhibitors, molecular dynamics simulations were performed, using an NMR structure of pentameric Aβ_{42} (PDB ID: 2BEG) [22]. A structure for EVVVKLF was generated through the "Builder" tool in PyMOL [23]. Molecular docking was performed through the automated protein docking server ClusPro [24-27]. The generated clusters were evaluated with the balanced scoring scheme. Following energy minimization, the interaction between Aβ_{42} key amyloid-forming segment ^{17}LVFFA^{21} (Fig 5A, dark grey) and EVVVKLF (Fig 5A, light grey) was ascertained (Fig 5A, left). Aβ_{42}+EVVVKLF complex structural stability was monitored through per-residue root mean square fluctuation (RMSF) calculation, as well as time-dependent root mean square

deviation (RMSD) measurements (Fig 5B and 5C, respectively). After 600 ns of molecular dynamics simulations, a complex dissociation has occurred, significantly changing the conformation of the pentamer, in comparison to its original state (Fig 5A). The C-termini of all five chains are characterized by large fluctuations (0.4 – 0.8 nm), with chains-A and -B exhibiting the highest mobility. In contrast, the N-termini of the aforementioned chains exhibit the lowest mobility among all chains, while the chain-E N-terminus is characterized by fluctuations of over 0.8 nm. Secondary structure analysis was performed using the dictionary of secondary structure of proteins (DSSP) algorithm [37,38] and reveals that *β*-sheet content gradually decreases (Fig 5D). Intermolecular hydrogen bonds are formed, even before the simulation has begun, and reach a maximum number of 12 (Fig 5E). Upon examination of the last frame of the simulation (Fig 5A, right), EVVVKLF has partly adopted a *β*-strand conformation. Using UCSF Chimera and the "FindHBond" tool [40], we show that EVVVKLF forms three possible hydrogen bonds with the chain-A ^{16}LVFFA^{21} region, becoming a part of an intermolecular β-sheet. EVVVKLF also forms hydrogen bonds with the C-terminus of the A-chain. By forming hydrogen bonds with both regions, it essentially "stitches" the N-terminal ^{17}LVFFA^{21} to the C-terminus. The fact that RMSF values are low for the N-terminus and high for the C-terminus hints that the latter moves towards the former. In this way, fibril elongation from chain-A could be blocked. The addition of more than one peptide-inhibitors could promote interactions with chain-E, effectively blocking both elongation epitopes of the pentamer.

Figure 5. Results of molecular dynamics simulations for Aβ_{42}+EVVVKLF. (A) First (0 ns, left) and last (600 ns, right) frames of the molecular dynamics simulation. The positions of the N- and C-terminals of each Aβ_{42} chain are marked on each frame (17.A-17.E and 42.A-42.E, respectively). EVVVKLF (light grey) forms hydrogen bonds (yellow lines) with the chain-A ^{17}LVFFA^{21} (dark grey), right after molecular docking and energy minimization. More bonds are formed by the end of the simulation. (B) RMSF per residue plot, after 600 ns of molecular dynamics simulations. (C) RMSD over time plot. (D) The total number of residues in *β*-sheets, according to DSSP, over time. (E) Number of intermolecular hydrogens bonds, between Aβ_{42} and EVVVKLF, over time.

Natively disordered regions in human clusterin α-chain

Human clusterin is believed to have three long molten globule-like regions [9]. PONDR® VLTX (http://www.pondr.com) predicts five natively disordered regions in clusterin α-chain (Fig 6), the longest of which is located at the C-terminus. All five aggregation prone regions are located near predicted natively disordered regions. ^{12}NFHAMFQ^{18} is on the right of the N-terminal natively disordered region and on a putative amphipathic *α*-helix [9]. Putative *α*-helices are believed to be implicated in the interaction between clusterin and its client proteins [9]. ^{30}AMDIHF^{35} is located directly to the right of said putative amphipathic *α*-helix. ^{81}ILSVD^{85} is surrounded by two natively disordered regions. ^{155}YYLRVTT^{161} is also located directly to the left of a natively disordered region, while ^{177}EVVVKLF^{183} is partly predicted as natively disordered. Interestingly, the EVVVKLF peptide-analogue adopts *β*-sheet secondary structure, according to the ATR FT-IR spectrum (Fig 3P). The proximity of all five aggregation-prone regions to natively disordered regions may hint that, due to the flexibility of the latter, the former could act semi-independently of the protein.

Figure 6. Predicted natively disordered regions, aggregation-prone regions, and putative amphipathic *α*-helices on human clusterin *α*-chain. All aggregation-prone regions are located near the predicted natively disordered regions. ^{12}NFHAMFQ^{18} is located on a putative amphipathic *α*-helix, while ^{177}EVVVKLF^{183} is partly predicted as natively disordered.

Discussion

Full-length clusterin could also have amyloidogenic properties *in vitro*

Recent studies have shown that short aggregation-prone segments, known as amyloidogenic determinants, can lead to amyloid formation, even when they are inserted in non-amyloidogenic proteins, via protein engineering [48]. The fact that clusterin has five such segments in its *α*-chain, provides potent indication that the *α*-chain and consequently the full-

length protein, may intrinsically exhibit amyloidogenicity. This argument has fascinating implications, especially considering clusterin's role as a molecular chaperone.

Molecular chaperones and their involvement in amyloid formation and inhibition

One of the fundamental functions of molecular chaperones is considered to be the prevention of protein aggregation and consequently, amyloid fibril formation [3]. Based on that notion, it has been suggested that molecular chaperones could be used as anti-amyloid drugs [49]. In direct contradiction to that, clusterin has the potential to form amyloid-like fibrils. In fact, there have been reports of other proteins that function as molecular chaperones and exhibit amyloidogenicity *in vitro* [5,6] or *in vivo* [4]. Despite lacking any sequence similarity, this group of proteins shares a significant number of similar features, besides having the potential to form amyloid-like fibrils.

A prominent example is α-crystallin, a small heat shock protein (sHSP), which is highly expressed in the eye lens. Full-length α-crystallin has been found to form amyloid-like fibrils *in vitro* [5] and is believed to be implicated in the formation of cataract [50]. As most sHSPs, α-crystallin exhibits remarkable structural plasticity, which is intertwined with its chaperone activity [51]. Interestingly, α-crystallin's chaperone activity is exhibited in a very similar manner to that of clusterin [52]. sHSPs exist in solution as oligomeric structures, ranging from 9 to 50 subunits. Those structures disassociate under stress and release functional subunits [53]. α-crystallin in particular, possesses a dynamic oligomeric structure, which, under increasing temperature, allows the exchange of subunits within proximate oligomers. The so-called "traveling subunits" are believed to play a fundamental role in α-crystallin's chaperone activity, by exposing hydrophobic surfaces and consequently, allowing hydrophobic interactions with misfolded proteins, including Aβ [54-56]. Even though this is the physiological mechanism in which α-crystallin functions, it is reminiscent of how amyloidogenic proteins behave on their way to self-

445 assembly and formation of amyloid fibrils [57]. This might explain the reports of *α*-crystallin
446 forming amyloid-like fibrils *in vitro [5]*.

447 Another relevant example is that of the caseins, a group of proteins that comprise the largest
448 part of the total protein content in milk [58] and are usually found in aggregates, known as
449 casein micelles. The micelles are primarily composed of four major proteins, namely α_{s1}-, α_{s2}-, *β*-
450 and *κ*-casein [59]. All four of them have been classified as intrinsically disordered proteins,
451 because of the considerable structural flexibility that they exhibit [60]. In consistence with
452 clusterin and *α*-crystallin, the major casein proteins are believed to function as molecular
453 chaperones [61], while *κ*-casein forms amyloid fibrils *in vitro* [6] and α_{s2}-casein forms amyloid
454 fibrils *in vivo*, in corpora amylacea, in the bovine mammary gland [2,4]. Yet, in physiological
455 conditions, α_{s1}-casein interacts with α_{s2}-casein, forming α_s-casein, effectively halting the
456 formation of amyloid fibrils [62]. Similarly, α_s-casein and *β*-casein inhibit *κ*-casein amyloid
457 formation, by shielding monomeric *κ*-casein hydrophobic surfaces with similar regions of their
458 respective sequences [63].

459 In summary, clusterin, *α*-crystallin, and the casein proteins share common features:

460 (1) They function as molecular chaperones, by exposing hydrophobic regions, interacting with and
461 stabilizing misfolded proteins on their way to aggregation.
462 (2) They show structural plasticity, either having molten globule-like or intrinsically disordered
463 regions on their sequence.
464 (3) They are found in solution as heterogeneous aggregates, oligomers, or micelles, which
465 dissociate under conditions of stress.
466 (4) They all interact with one, or more amyloidogenic proteins.
467 (5) Parts of their sequence, or the full-length proteins, are known to form amyloid-like fibrils *in*
468 *vitro* or *in vivo*.

These similarities may underlie a common mechanism in which the cell prevents toxic amyloid formation under different conditions of stress, by utilizing the intrinsic amyloidogenicity of specific molecular chaperones. For clusterin, amyloidogenesis inhibition could be activated under pH-induced stress and achieved through the interaction of its aggregation-prone regions with amyloidogenic proteins, on their way to aggregation. Likewise, α-crystallin could act under temperature-induced stress and the casein proteins may present a more specific system of amyloid inhibition, present primarily at the mammary gland.

A putative mechanism for clusterin-mediated inhibition of Aβ amyloidogenesis

Clusterin α-chain peptide-analogues can inhibit Aβ amyloidogenesis *in vitro*, and the structural flexibility that natively disordered regions introduce, may enable them to act semi-independently of the protein. Having established that, we opted to propose a mechanism in which clusterin could use its aggregation-prone regions to exert its molecular chaperone activity on Aβ.

It is believed that Aβ amyloidogenesis is promoted by acidic pH [64]. As previously mentioned, mildly acidic pH also allows the disassociation of clusterin's heterogeneous aggregates, releasing chaperone-active subunits [10]. In its disassociated form, clusterin is assumed to hydrophobically interact with its client-proteins through amphipathic α-helices, which are surrounded by molten globule-like regions [9]. ^{12}NFHAMFQ^{18}, one of clusterin's aggregation-prone regions, is located on a putative amphipathic α-helix. However, we have already proved that NFHAMFQ also has the propensity to form β-strands [7], hinting that the broader region has the intrinsic conformational properties of a chameleon sequence. When in proximity with an Aβ fibril, the α-helical ^{12}NFHAMFQ^{18} could unfold and then refold into a β-strand, allowing interaction with Aβ's β-stranded regions and temporarily halting fibril growth. This process could trigger the exposition of clusterin's other aggregation-prone regions and allow it to attach itself at the edge of the Aβ fibril, via β-strand hydrogen bonding. In this manner, it would not allow Aβ monomers to elongate the fibril, effectively blocking further polymerization. At the

same time, free clusterin subunits could bind to Aβ monomers, forming complexes and stabilizing their structure, until it passes the baton to other molecular chaperones, once again, halting fiber growth and minimizing the possibility of toxic secondary nucleation [65]. The suggested mechanism is visualized in Fig 7.

Figure 7. Putative mechanism of clusterin-mediated inhibition of Aβ amyloidogenesis. (1) Under acidic pH-induced stress, Aβ may partially unfold, exposing hydrophobic regions with the propensity to form β-strands. At the same time, the acidic pH triggers the disassociation of clusterin's heterogeneous aggregates. (2) Misfolded Aβ begin to form amyloid fibrils, but (3) the disassociated clusterin subunits (CLU) halt fibril growth, utilizing their aggregation-prone regions, which tend to form β-strands as well. The outlined picture is derived from the last frame of the molecular dynamics simulation of $A\beta_{42}$+EVVVKLF. (4) Clusterin binds misfolded Aβ monomers, forming complexes and stabilizes their structure, until (5) they are refolded by other molecular chaperones. (6) In case misfolded Aβ species are produced faster than clusterin can stabilize their structure, it essentially brings them into proximity with remote monomers, accelerating amyloid formation.

The putative mechanism that was just described, is also supported by the identification of a pathological mutation on clusterin's gene, in AD patients. As previously mentioned, p.I360N changes the aggregation-prone region ^{81}ILSVD^{85} to ^{81}NLSVD^{85} [44]. Considering that out of the peptides we examined, ILSVD is hinted to be one of the better Aβ fibril formation inhibitors, this mutation could lead to a malfunction in the clusterin-mediated amyloidogenesis inhibition system. Thus, the pathogenicity of the phenotype could be explained by clusterin's inability to inhibit amyloid formation, due to the absence of its most aggregation-prone region, that being ^{81}ILSVD^{85}, which would normally inhibit Aβ fibril formation.

The aforementioned mechanism can explain why clusterin is found co-localized with Aβ fibrillar deposits [12] and is consistent with reports of clusterin decelerating Aβ fibril formation [65,66]. However, clusterin's occasional contribution to the appearance of AD symptoms [15,16] needs further elucidation. It is logical to assume that, when Aβ misfolded monomers are produced

faster than what clusterin's existing population can process, the resulting complexes would fail to stabilize A*β*'s structure, essentially bringing remote misfolded monomers into proximity. This could accelerate amyloid fibril formation (Fig 6 – 6), while clusterin would end up co-localized with the fibrillar deposits. This hypothesis is supported by the findings of Yerbury *et al*., which show that clusterin's enhancing effect on amyloid formation is caused by a low clusterin:substrate ratio [45]. A relevant example could be found in patients with familial Alzheimer's disease (FAD), where A*β* is produced much faster than usual [67]. In fact, most pre-clinical studies on AD use FAD animals as models, because it is a guaranteed method of acquiring early-onset AD test subjects [68]. This could also be the case for Oh *et. al*, who showed that clusterin-null 5XFAD mice, show AD symptoms later than their littermate counterparts [15]. In the end, molecular chaperone-mediated amyloidogenesis inhibition, seems to be a double-edged sword for the cell, effective, but at the same time, conditionally harmful. The inadvertent bias that pre-clinical studies introduce, using test subjects with FAD, rather than sporadic AD, could make the inhibition system seem much more flawed than it really is.

Peptide-based amyloidogenesis inhibitors, derived from aggregation-prone protein regions

We ultimately proposed that the cell can prevent amyloid formation by utilizing the intrinsic amyloidogenicity of specific molecular chaperones, similar to how functional amyloids work. If that statement proves to be true, harnessing the ability of molecular chaperones to halt amyloid formation could be essential to tackling AD and other amyloidoses. The key to inhibiting amyloid formation lies in the aggregation-prone regions of said proteins, thus synthesizing and studying peptides from such regions could provide novel inhibitors of A*β* amyloidogenesis and amyloid formation in general [69].

It is worth mentioning that, the ability of molecular chaperones to inhibit amyloid formation doesn't seem to be substrate-specific, meaning that one chaperone could act as an amyloidogenesis inhibitor for a variety of different amyloidogenic proteins, even if they are not

known to interact *in vivo*. For example, though α-crystallin is known to interact with Aβ [56], the casein proteins are not. Despite that, all of them can inhibit Aβ amyloidogenesis *in vitro [70,71]*. Furthermore, this also seems to be the case for aggregation-prone peptides that are not derived from regions of molecular chaperones [46]. Mimicking the physiological system for amyloidogenesis prevention and extending it to aggregation-prone peptide-analogues of non-chaperone-active proteins could provide us with a much greater variety of potential inhibitors.

Despite the potential that specific peptides show as amyloidogenesis inhibitors, it is of vital importance to ensure that they are non-toxic for the cell. It is noteworthy that, even though some molecular chaperones have amyloidogenic properties, they seem to not have negative effects on the survival of the cell. In a similar manner, functional amyloids are not harmful to the organisms in which they appear. It is believed that controlling the expression of amyloidogenic proteins, regulating fibril formation with co-localized proteins-molecules, and the fact that they are often found isolated inside membrane-bound compartments, are some of the reasons why functional amyloids are not toxic [72]. For the peptide-inhibitors to be usable, these questions must be accurately answered, and the findings should be incorporated in their implementation as potential drugs for amyloidoses, especially when it comes to peptide concentration and the complementary substances that should be administered.

Limitations

It can be inferred that there are no clear experimental data that connect the inhibitory effect of the peptide-analogues on Aβ fibril formation and the inhibition associated with the full-length protein. However, there are enough indications that support our hypothesis, which makes us confident that the proposed mechanism stands to reason. The most striking example is that of the p.I360N mutation, which has been identified in a patient with AD and changes the aggregation-prone region ^{81}ILSVD^{85} to ^{81}NLSVD^{85}. The resulting mutant is stripped of its most aggregation-prone region, which corresponds to one of the most potent peptide-inhibitors we

showcased. Furthermore, bibliographic data reveal that clusterin may not be the only molecular chaperone to prevent protein aggregation by utilizing aggregation-prone regions of its sequence. On the contrary, it belongs to a group of proteins with similar function. Unfortunately, studying the molecular interactions of these proteins with their substrates may prove hard. Clusterin, in particular, is infamously difficult to purify and biophysically characterize, making the specifics of its structure and function a true mystery. We are hopeful that our findings will provide a fresh point of view and future studies will shed light on all the details that remain unclear.

There are no concerns over the statistical integrity of our study, considering that it only involves replicable *in vitro* and computational data.

Conclusions

Clusterin has at least five aggregation-prone regions in its α-chain and these regions have an essential role in the inhibition of amyloid-β fibril formation. These findings hint that molecular chaperones with amyloidogenic properties might be implicated in the regulation of amyloid formation, essentially acting as functional amyloids. Harnessing the ability of molecular chaperones to halt amyloid formation could be of vital importance for the treatment of Alzheimer's disease and other amyloidoses.

Abbreviations

Aβ: Amyloid-β

AD: Alzheimer's Disease

ATP: Adenosine Triphosphate

ATR FT-IR: Attenuated Total Reflectance Fourier Transform Infrared

CLU: Clusterin

FAD: Familial Alzheimer's Disease

HFIP: 1,1,1,3,3,3-Hexafluoro-2-propanol

MP: Misfolded Proteins

NP: Native Proteins

RMSD: Root Mean Square Deviation

RMSF: Root Mean Square Fluctuation

sHSP: small Heat Shock Protein

TEM: Transmission Electron Microscopy

ThT: Thioflavin T

Declarations

Ethics approval and consent to participate: Not applicable

Consent for publication: All authors have approved the contents of this manuscript and provided consent for publication.

Availability of data and materials: The datasets used and/or analyzed during the current study are available from the corresponding author on reasonable request.

Competing interests: The authors declare no conflicts of interest.

Funding: This research has been co-financed by the European Union and Greek national funds through the Operational Program "Competitiveness, Entrepreneurship and Innovation", under the call "RESEARCH – CREATE – INNOVATE" (project code: T1EDK-00353).

Authors' contributions: P.M.S. performed sample preparation, Congo Red birefringence and ThT kinetics assays, acquired and processed TEM, X-ray diffraction, and ATR FT-IR spectroscopy data, analyzed the molecular dynamics simulations results, helped in conceiving the project, and wrote the initial draft of the manuscript. G.I.N. participated and assisted in all the experiments. P.L.T. co-supervised and helped in conceiving the project. M.K.T. performed the molecular dynamics simulations and participated in the analysis of the results. N.C.P. supervised the

molecular dynamics simulations. A. H. co-supervised the TEM experiments. I.P.T. helped in conceiving the project and supervised the ThT kinetics assay. V.A.I. supervised and helped in conceiving the project. All authors discussed the results and edited or commented on the manuscript.

Acknowledgments: We acknowledge support of this work by the project "INSPIRED-The National Research Infrastructures on Integrated Structural Biology, Drug Screening Efforts and Drug target functional characterization" (MIS 5002550) which is implemented under the Action "Reinforcement of the Research and Innovation Infrastructure", funded by the Operational Program "Competitiveness, Entrepreneurship and Innovation" (NSRF 2014-2020) and co-funded by Greece and the European Union (European Regional Development Fund). The molecular dynamics simulations were performed utilizing computational time granted from the Greek Research & Technology Network (GRNET) at the National HPC facility – ARIS under project ID "PR007003-AbetaDynamics". We also acknowledge Dr. George Baltatzis for kindly assisting us with handling the Morgagni Microscope at the 1st Department of Pathology, Medical School, National and Kapodistrian University of Athens. Finally, we acknowledge the support of Dr. Aimilia Sklirou, who kindly assisted with handling the Tecan Spark microplate reader.

References

1. Kyle RA. Amyloidosis: a brief history. Amyloid : the international journal of experimental and clinical investigation : the official journal of the International Society of Amyloidosis. 2011 Jun;18 Suppl 1:6-7.
2. Benson MD, Buxbaum JN, Eisenberg DS, et al. Amyloid nomenclature 2020: update and recommendations by the International Society of Amyloidosis (ISA) nomenclature committee. Amyloid : the international journal of experimental and clinical investigation : the official journal of the International Society of Amyloidosis. 2020 Dec;27(4):217-222.

3. Wentink A, Nussbaum-Krammer C, Bukau B. Modulation of Amyloid States by Molecular Chaperones. Cold Spring Harbor perspectives in biology. 2019 Feb 12.
4. Niewold TA, Murphy CL, Hulskamp-Koch CA, et al. Casein related amyloid, characterization of a new and unique amyloid protein isolated from bovine corpora amylacea. Amyloid : the international journal of experimental and clinical investigation : the official journal of the International Society of Amyloidosis. 1999 Dec;6(4):244-9.
5. Ecroyd H, Carver JA. Crystallin proteins and amyloid fibrils. Cellular and molecular life sciences : CMLS. 2009 Jan;66(1):62-81.
6. Ecroyd H, Thorn DC, Liu Y, et al. The dissociated form of kappa-casein is the precursor to its amyloid fibril formation. The Biochemical journal. 2010 Jul 15;429(2):251-60.
7. Tsiolaki PL, Nastou KC, Louros NN, et al. Exploring Amyloidogenicity of Clusterin: A Structural and Bioinformatics Analysis. Advances in experimental medicine and biology. 2017;989:93-107.
8. Jones SE, Jomary C. Clusterin. The international journal of biochemistry & cell biology. 2002 May;34(5):427-31.
9. Bailey RW, Dunker AK, Brown CJ, et al. Clusterin, a binding protein with a molten globule-like region. Biochemistry. 2001 Oct 2;40(39):11828-40.
10. Poon S, Rybchyn MS, Easterbrook-Smith SB, et al. Mildly acidic pH activates the extracellular molecular chaperone clusterin. The Journal of biological chemistry. 2002 Oct 18;277(42):39532-40.
11. Poon S, Easterbrook-Smith SB, Rybchyn MS, et al. Clusterin is an ATP-independent chaperone with very broad substrate specificity that stabilizes stressed proteins in a folding-competent state. Biochemistry. 2000 Dec 26;39(51):15953-60.
12. Calero M, Rostagno A, Frangione B, et al. Clusterin and Alzheimer's disease. Sub-cellular biochemistry. 2005;38:273-98.

669 13. Rohne P, Prochnow H, Koch-Brandt C. The CLU-files: disentanglement of a mystery.
670 Biomolecular concepts. 2016 Feb;7(1):1-15.
671 14. Matsubara E, Soto C, Governale S, et al. Apolipoprotein J and Alzheimer's amyloid beta
672 solubility. The Biochemical journal. 1996 Jun 1;316 (Pt 2):671-9.
673 15. Oh SB, Kim MS, Park S, et al. Clusterin contributes to early stage of Alzheimer's disease
674 pathogenesis. Brain pathology. 2019 Mar;29(2):217-231.
675 16. DeMattos RB, O'Dell M A, Parsadanian M, et al. Clusterin promotes amyloid plaque
676 formation and is critical for neuritic toxicity in a mouse model of Alzheimer's disease.
677 Proceedings of the National Academy of Sciences of the United States of America. 2002
678 Aug 6;99(16):10843-8.
679 17. Nastou KC, Nasi GI, Tsiolaki PL, et al. AmyCo: the amyloidoses collection. Amyloid : the
680 international journal of experimental and clinical investigation : the official journal of
681 the International Society of Amyloidosis. 2019 Sep;26(3):112-117.
682 18. Frousios KK, Iconomidou VA, Karletidi CM, et al. Amyloidogenic determinants are usually
683 not buried. BMC structural biology. 2009 Jul 9;9:44.
684 19. CrysAlis^{PRO}. Agilent Technologies [Software system]. Version 1.171.37.31. Oxford, UK:
685 Agilent Technologies UK Ltd; 2014. Software system.
686 20. Battye TG, Kontogiannis L, Johnson O, et al. iMOSFLM: a new graphical interface for
687 diffraction-image processing with MOSFLM [Research Support, Non-U.S. Gov't]. Acta
688 crystallographica Section D, Biological crystallography. 2011 Apr;67(Pt 4):271-81.
689 21. Savitzky A, Golay MJE. Smoothing and Differentiation of Data by Simplified Least
690 Squares Procedures. Analytical Chemistry. 1964 1964/07/01;36(8):1627-1639.
691 22. Luhrs T, Ritter C, Adrian M, et al. 3D structure of Alzheimer's amyloid-beta(1-42) fibrils.
692 Proceedings of the National Academy of Sciences of the United States of America. 2005
693 Nov 29;102(48):17342-7.

694 23. Delano WL. The PyMOL Molecular Graphics System. 400, Oyster Point Blvd., Suite 213,
695 South San Francisco, CA 94080-1918, USA: DeLano Scientific LLC
696 2005.
697 24. Kozakov D, Beglov D, Bohnuud T, et al. How good is automated protein docking?
698 Proteins. 2013 Dec;81(12):2159-66.
699 25. Kozakov D, Hall DR, Xia B, et al. The ClusPro web server for protein-protein docking. Nat
700 Protoc. 2017 Feb;12(2):255-278.
701 26. Porter KA, Xia B, Beglov D, et al. ClusPro PeptiDock: efficient global docking of peptide
702 recognition motifs using FFT. Bioinformatics. 2017 Oct 15;33(20):3299-3301.
703 27. Vajda S, Yueh C, Beglov D, et al. New additions to the ClusPro server motivated by
704 CAPRI. Proteins. 2017 Mar;85(3):435-444.
705 28. Kutzner C, Pall S, Fechner M, et al. More bang for your buck: Improved use of GPU nodes
706 for GROMACS 2018. J Comput Chem. 2019 Oct 15;40(27):2418-2431.
707 29. Lindorff-Larsen K, Piana S, Palmo K, et al. Improved side-chain torsion potentials for the
708 Amber ff99SB protein force field. Proteins. 2010 Jun;78(8):1950-8.
709 30. Jorgensen WL, Chandrasekhar, J., Madura, J. D., Impey, R. W., & Klein, M. L. Comparison
710 of simple potential functions for simulating liquid water. The Journal of Chemical
711 Physics. 1983;79(2).
712 31. Berendsen HJC, Postma, J. P. M., Van Gunsteren, W. F., Dinola, A., & Haak, J. R.
713 Molecular dynamics with coupling to an external bath. The Journal of Chemical Physics.
714 1984;81(8).
715 32. Berendsen HJC. Transport Properties Computed by Linear Response through Weak
716 Coupling to a Bath. Computer Simulation in Materials Science. Vol. 205: Springer,
717 Dordrecht; 1991. p. 139-155.

33. Berk Hess HB, Herman J. C. Berendsen, Johannes G. E. M. Fraaije. LINCS: A linear constraint solver for molecular simulations. Journal of Computational Chemistry. 1997;18(12):1463-1472.

34. Essmann U, Perera, L., Berkowitz, M. L., Darden, T., Lee, H., & Pedersen, L. G. A smooth particle mesh Ewald method. The Journal of Chemical Physics 1995;103.

35. Humphrey W, Dalke A, Schulten K. VMD: visual molecular dynamics. J Mol Graph. 1996 Feb;14(1):33-8, 27-8.

36. Maiorov VN, Crippen GM. Size-independent comparison of protein three-dimensional structures. Proteins: Structure, Function, and Genetics. 1995;22(3):273-283.

37. Kabsch W, Sander C. Dictionary of protein secondary structure: pattern recognition of hydrogen-bonded and geometrical features. Biopolymers. 1983 Dec;22(12):2577-637.

38. Touw WG, Baakman C, Black J, et al. A series of PDB-related databanks for everyday needs. Nucleic Acids Research. 2015;43(D1):D364-D368.

39. van der Spoel D, van Maaren PJ, Larsson P, et al. Thermodynamics of Hydrogen Bonding in Hydrophilic and Hydrophobic Media. The Journal of Physical Chemistry B. 2006;110(9):4393-4398.

40. Pettersen EF, Goddard TD, Huang CC, et al. UCSF Chimera?A visualization system for exploratory research and analysis. Journal of Computational Chemistry. 2004;25(13):1605-1612.

41. Sunde M, Blake CC. From the globular to the fibrous state: protein structure and structural conversion in amyloid formation. Quarterly reviews of biophysics. 1998 Feb;31(1):1-39.

42. Makin OS, Serpell LC. X-ray diffraction studies of amyloid structure. Methods in molecular biology. 2005;299:67-80.

742 43. Surewicz WK, Mantsch HH, Chapman D. Determination of protein secondary structure
743 by Fourier transform infrared spectroscopy: a critical assessment. Biochemistry. 1993
744 Jan 19;32(2):389-94.
745 44. Bettens K, Vermeulen S, Van Cauwenberghe C, et al. Reduced secreted clusterin as a
746 mechanism for Alzheimer-associated CLU mutations. Molecular neurodegeneration.
747 2015 Jul 16;10:30.
748 45. Yerbury JJ, Poon S, Meehan S, et al. The extracellular chaperone clusterin influences
749 amyloid formation and toxicity by interacting with prefibrillar structures. FASEB journal :
750 official publication of the Federation of American Societies for Experimental Biology.
751 2007 Aug;21(10):2312-22.
752 46. Lu J, Cao Q, Wang C, et al. Structure-Based Peptide Inhibitor Design of Amyloid-beta
753 Aggregation. Frontiers in molecular neuroscience. 2019;12:54.
754 47. Chafekar SM, Malda H, Merkx M, et al. Branched KLVFF tetramers strongly potentiate
755 inhibition of beta-amyloid aggregation. Chembiochem. 2007 Oct 15;8(15):1857-64.
756 48. Teng PK, Eisenberg D. Short protein segments can drive a non-fibrillizing protein into the
757 amyloid state. Protein engineering, design & selection : PEDS. 2009 Aug;22(8):531-6.
758 49. Yerbury JJ, Kumita JR. Protein chemistry of amyloid fibrils and chaperones: implications
759 for amyloid formation and disease. Current Chemical Biology. 2010;4(2):89-98.
760 50. Meehan S, Berry Y, Luisi B, et al. Amyloid fibril formation by lens crystallin proteins and
761 its implications for cataract formation. The Journal of biological chemistry. 2004 Jan
762 30;279(5):3413-9.
763 51. Basha E, O'Neill H, Vierling E. Small heat shock proteins and alpha-crystallins: dynamic
764 proteins with flexible functions. Trends in biochemical sciences. 2012 Mar;37(3):106-17.
765 52. Carver JA, Rekas A, Thorn DC, et al. Small heat-shock proteins and clusterin: intra- and
766 extracellular molecular chaperones with a common mechanism of action and function?
767 IUBMB life. 2003 Dec;55(12):661-8.

768 53. Haslbeck M, Buchner J. Chaperone function of sHsps. Progress in molecular and
769 subcellular biology. 2002;28:37-59.
770 54. Inoue R, Takata T, Fujii N, et al. New insight into the dynamical system of alphaB-
771 crystallin oligomers. Scientific reports. 2016 Jul 6;6:29208.
772 55. Doss EW, Ward KA, Koretz JF. Preliminary studies on the aggregation process of alpha-
773 crystallin. Experimental eye research. 1997 Aug;65(2):255-66.
774 56. Narayan P, Meehan S, Carver JA, et al. Amyloid-beta oligomers are sequestered by both
775 intracellular and extracellular chaperones. Biochemistry. 2012 Nov 20;51(46):9270-6.
776 57. Cheon M, Chang I, Mohanty S, et al. Structural reorganisation and potential toxicity of
777 oligomeric species formed during the assembly of amyloid fibrils. PLoS computational
778 biology. 2007 Sep;3(9):1727-38.
779 58. Kunz C, Lonnerdal B. Human-milk proteins: analysis of casein and casein subunits by
780 anion-exchange chromatography, gel electrophoresis, and specific staining methods.
781 The American journal of clinical nutrition. 1990 Jan;51(1):37-46.
782 59. McMahon DJ, Oommen BS. Supramolecular structure of the casein micelle. Journal of
783 dairy science. 2008 May;91(5):1709-21.
784 60. Redwan EM, Xue B, Almehdar HA, et al. Disorder in milk proteins: caseins, intrinsically
785 disordered colloids. Current protein & peptide science. 2015;16(3):228-42.
786 61. Morgan PE, Treweek TM, Lindner RA, et al. Casein proteins as molecular chaperones.
787 Journal of agricultural and food chemistry. 2005 Apr 6;53(7):2670-83.
788 62. Thorn DC, Ecroyd H, Sunde M, et al. Amyloid fibril formation by bovine milk alpha s2-
789 casein occurs under physiological conditions yet is prevented by its natural counterpart,
790 alpha s1-casein. Biochemistry. 2008 Mar 25;47(12):3926-36.
791 63. Thorn DC, Meehan S, Sunde M, et al. Amyloid fibril formation by bovine milk kappa-
792 casein and its inhibition by the molecular chaperones alphaS- and beta-casein.
793 Biochemistry. 2005 Dec 27;44(51):17027-36.

64. Su Y, Chang PT. Acidic pH promotes the formation of toxic fibrils from beta-amyloid peptide. Brain research. 2001 Mar 2;893(1-2):287-91.

65. Beeg M, Stravalaci M, Romeo M, et al. Clusterin Binds to Abeta1-42 Oligomers with High Affinity and Interferes with Peptide Aggregation by Inhibiting Primary and Secondary Nucleation. The Journal of biological chemistry. 2016 Mar 25;291(13):6958-66.

66. de Retana SF, Marazuela P, Sole M, et al. Peripheral administration of human recombinant ApoJ/clusterin modulates brain beta-amyloid levels in APP23 mice. Alzheimer's research & therapy. 2019 May 10;11(1):42.

67. Wu L, Rosa-Neto P, Hsiung GY, et al. Early-onset familial Alzheimer's disease (EOFAD). The Canadian journal of neurological sciences Le journal canadien des sciences neurologiques. 2012 Jul;39(4):436-45.

68. LaFerla FM, Green KN. Animal models of Alzheimer disease. Cold Spring Harbor perspectives in medicine. 2012 Nov 1;2(11).

69. Connelly S, Choi S, Johnson SM, et al. Structure-based design of kinetic stabilizers that ameliorate the transthyretin amyloidoses. Current opinion in structural biology. 2010 Feb;20(1):54-62.

70. Carrotta R, Canale C, Diaspro A, et al. Inhibiting effect of alpha(s1)-casein on Abeta(1-40) fibrillogenesis. Biochimica et biophysica acta. 2012 Feb;1820(2):124-32.

71. Raman B, Ban T, Sakai M, et al. AlphaB-crystallin, a small heat-shock protein, prevents the amyloid fibril growth of an amyloid beta-peptide and beta2-microglobulin. The Biochemical journal. 2005 Dec 15;392(Pt 3):573-81.

72. Jackson MP, Hewitt EW. Why are Functional Amyloids Non-Toxic in Humans? Biomolecules. 2017 Sep 22;7(4).

Figures

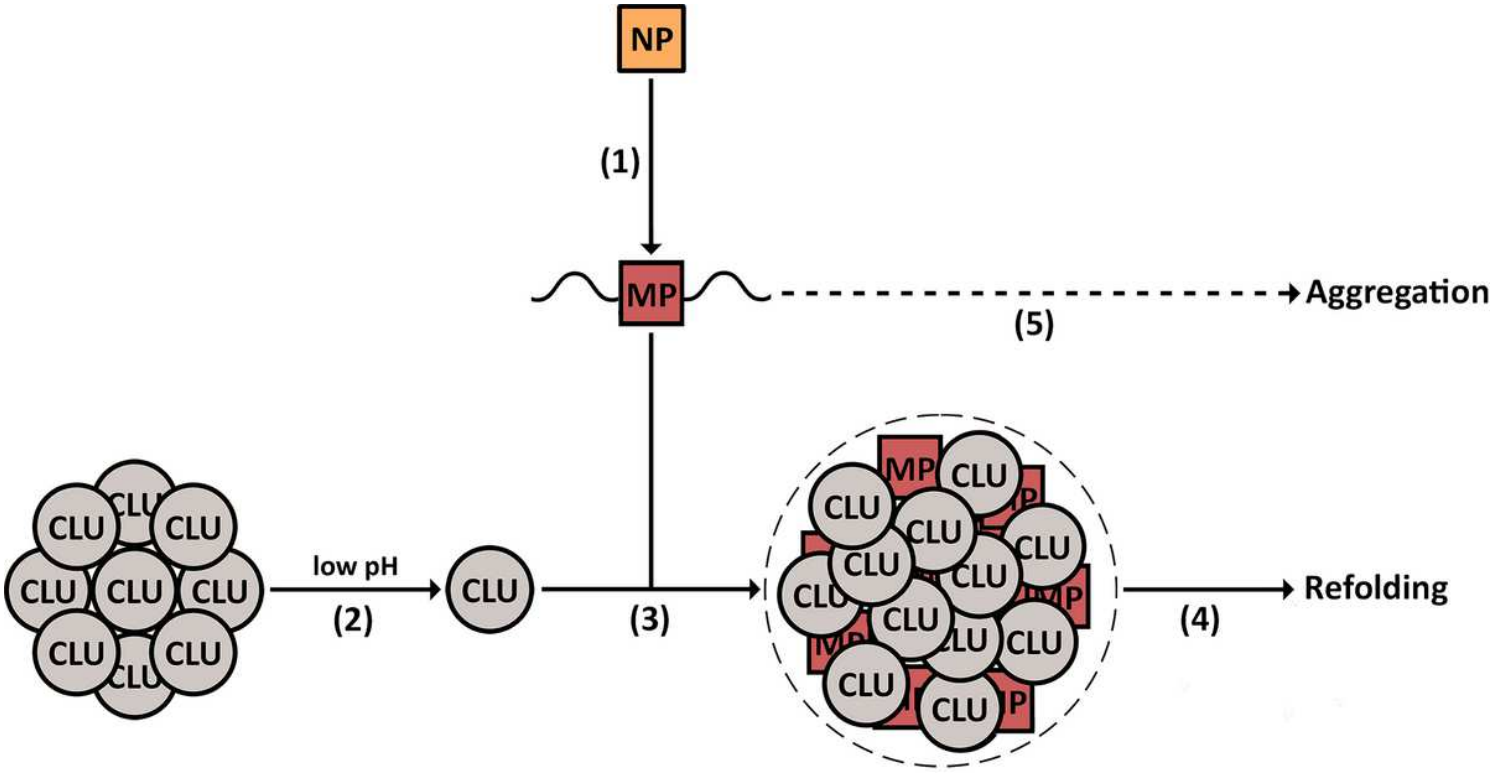

Figure 1

Representation of clusterin's molecular chaperone activity. (1) Under stress (low pH), native proteins (NP) may partially unfold and become misfolded. (2) At slightly acidic pH, clusterin's (CLU) oligomers start disassociating and the chaperone-active clusterin subunits get released. (3) The free clusterin subunits bind the misfolded proteins (MP) and form a complex, effectively stabilizing them, (4) while other molecular chaperones refold them to their native state. (5) If this mechanism proves ineffective, the misfolded proteins may form aggregates.

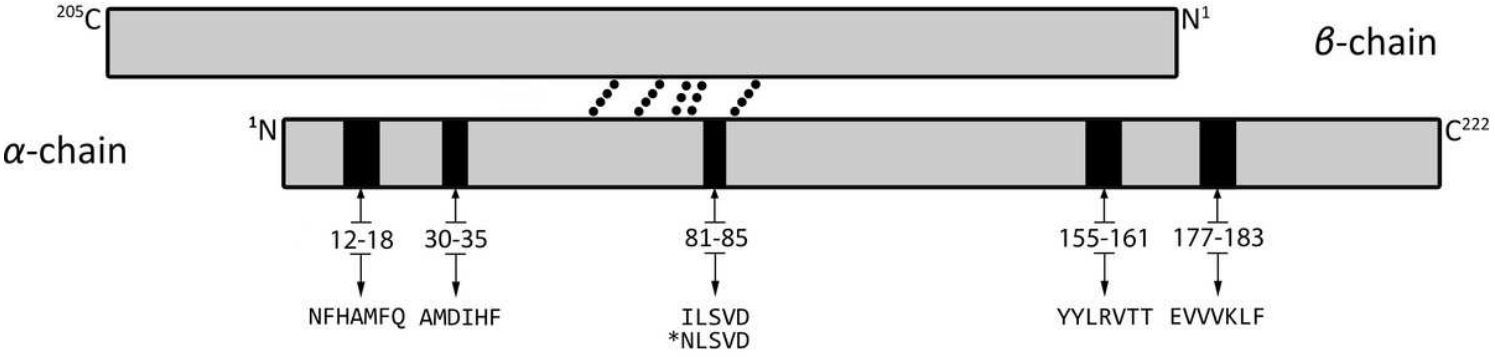

Figure 2

A simple representation of clusterin's two chains. Each chain is colored grey, with a black outline, and its sequence is numbered as found in the mature protein. The α-chain consists of 222 amino acid residues.

The β-chain is slightly shorter, consisting of 205 amino acid residues. The two chains are joined by five disulfide bonds, depicted as black dots. The aggregation-prone regions of the α-chain are depicted as black rectangles on clusterin's sequence.

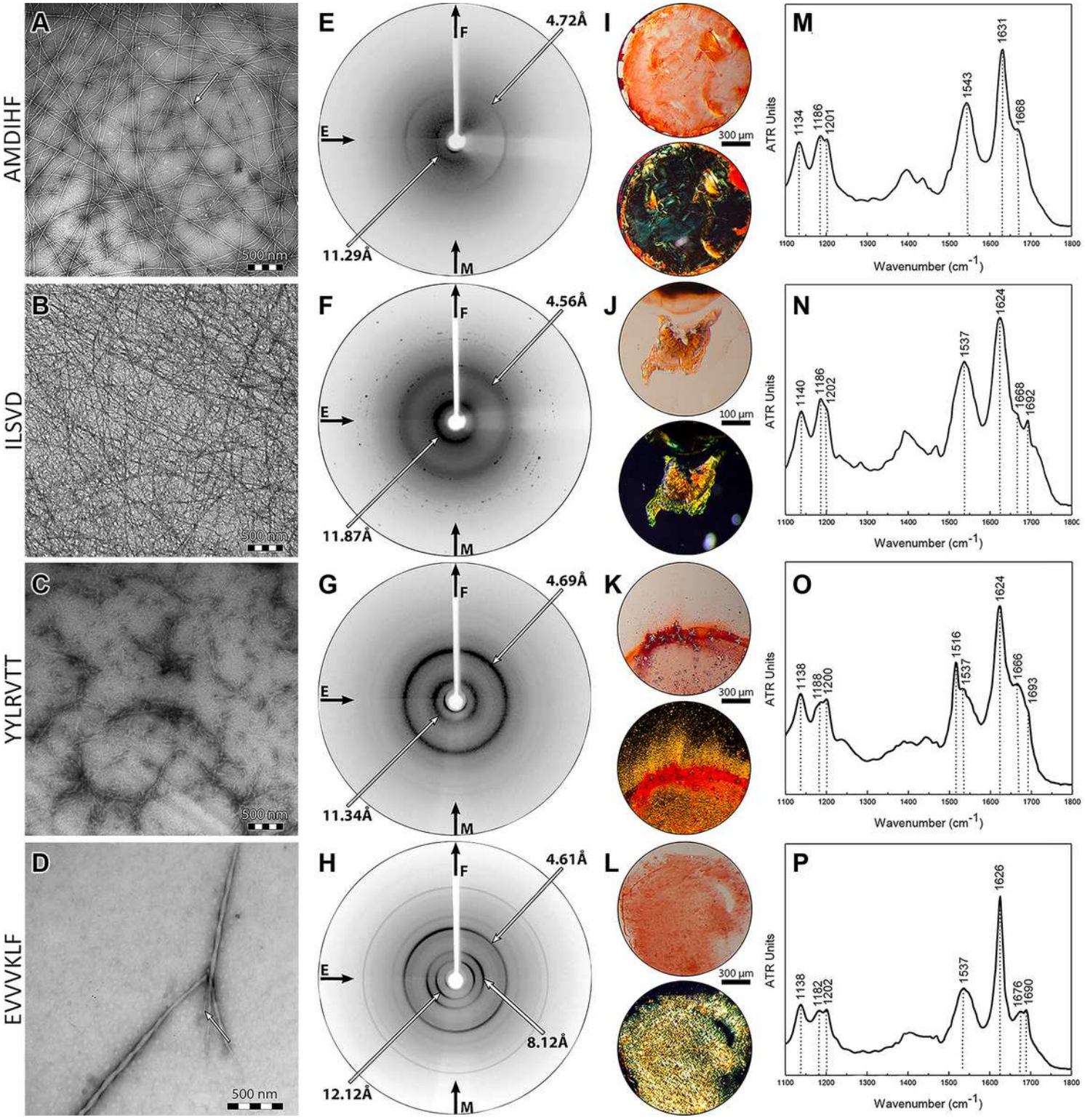

Figure 3

All the peptide-analogues fulfill the experimental criteria. (A-D) Transmission electron micrographs of amyloid-like fibrils derived from 500 µm solutions of peptides AMDIHF, ILSVD, YYLRVTT, and EVVVKLF,

respectively. White arrows mark single fibrils with the diameter of typical amyloid fibrils. (E-H) X-ray diffraction patterns of oriented fibers, derived from 1 mM solutions of the four peptides, respectively. Reflections marked with arrows are indicative of the “cross-β” structure, which amyloids typically have. (I-L) Photomicrographs of gels, derived from 500 μM solutions of the four peptides, respectively. Congo red is bound, as seen under bright field illumination (upper). The apple-green birefringence that amyloids typically exhibit is observed under crossed polars (lower). (M-P) ATR FT-IR spectra (1100–1800 cm-1) produced from thin hydrated films created by 500 μM solutions of the four peptides, respectively. Fibrils derived from each peptide have a β-sheet secondary structure, as hinted by the presence of strong amide I and II bands.

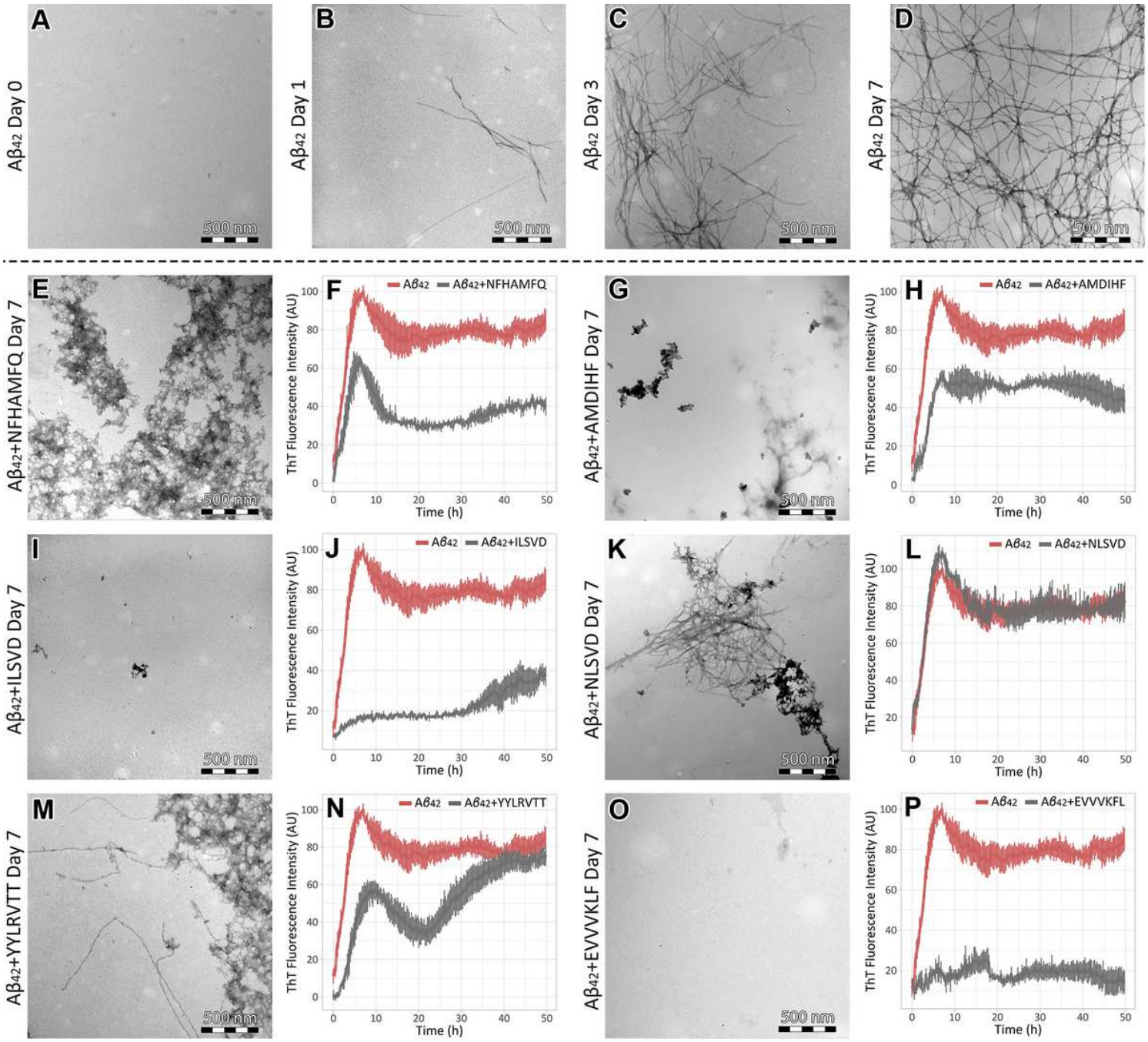

Figure 4

Clusterin peptide-analogues inhibit or delay Aβ42 fibril formation. (A-D) Transmission electron micrographs of Aβ42, incubated for 0, 1, 3, and 7 days, respectively. Amyloid fibrils are observed from day 1 to day 7. The number of fibrils raises as incubation time increases. (E, F) Transmission electron micrograph and ThT fluorescence emission spectrum of Aβ42 co-incubated with NFHAMFQ for 7 days and over a period of 50 hours, respectively. (G, H) Transmission electron micrograph and ThT fluorescence emission spectrum of Aβ42 co-incubated with AMDIHF for 7 days and over a period of 50 hours, respectively. (I, J) Transmission electron micrograph and ThT fluorescence emission spectrum of Aβ42 co-incubated with ILSVD for 7 days and over a period of 50 hours, respectively. (K, L) Transmission electron micrograph and ThT fluorescence emission spectrum of Aβ42 co-incubated with the mutant peptide, NLSVD, for 7 days and over a period of 50 hours, respectively. (M, N) Transmission electron micrograph and ThT fluorescence emission spectrum of Aβ42 co-incubated with YYLRVTT for 7 days and over a period of 50 hours, respectively. (O, P) Transmission electron micrograph and ThT fluorescence emission spectrum of Aβ42 co-incubated with EVVVKLF for 7 days and over a period of 50 hours, respectively. Error bars in ThT fluorescence emission spectra represent standard deviation among triplicates. TEM experiments contained 100 μM Aβ42 and 100 μM clusterin peptide-analogues, while ThT experiments contained 10 μM and 10 μM, respectively.

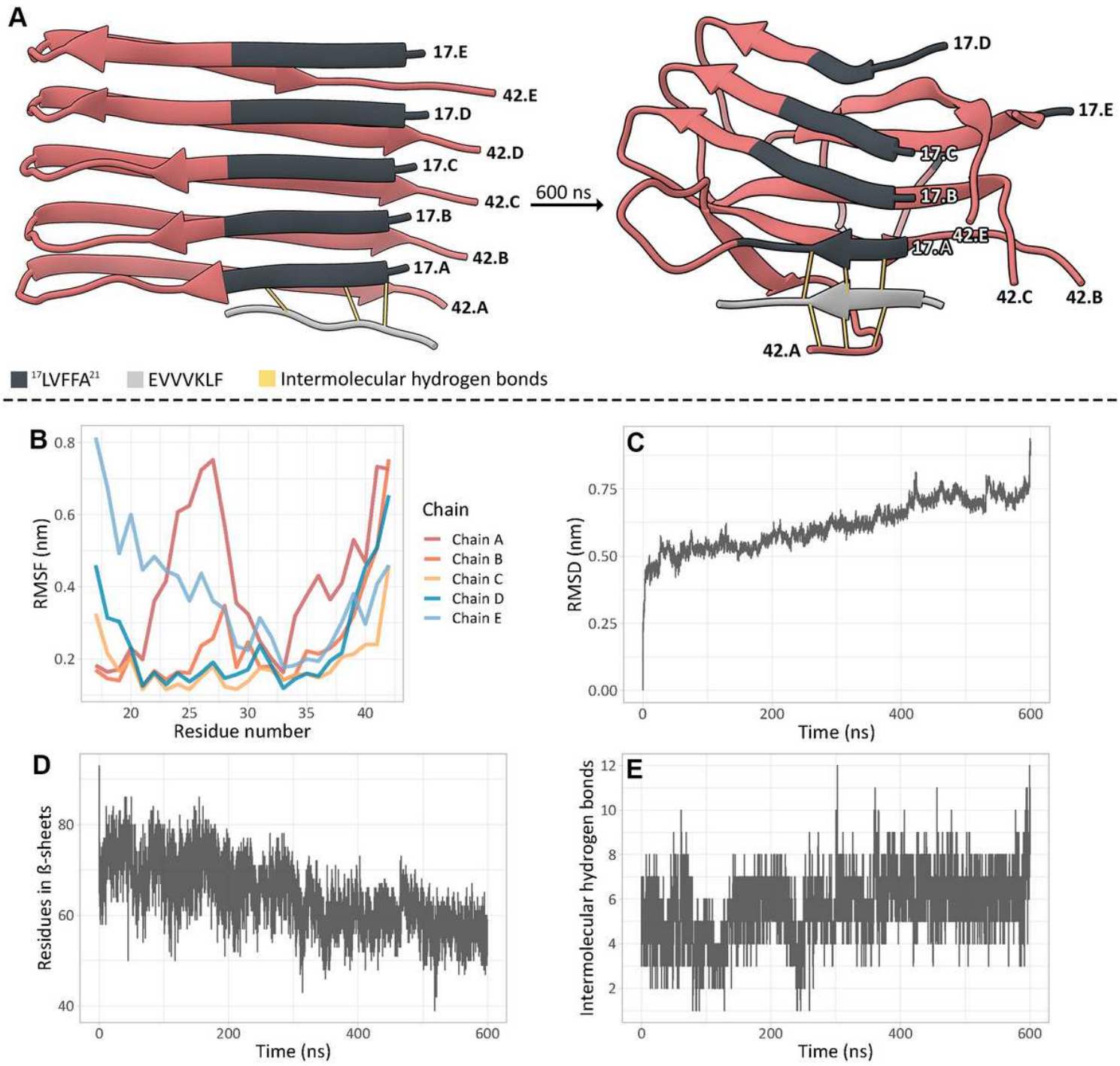

Figure 5

Results of molecular dynamics simulations for Aβ42+EVVVKLF. (A) First (0 ns, left) and last (600 ns, right) frames of the molecular dynamics simulation. The positions of the N- and C-terminals of each Aβ42 chain are marked on each frame (17.A-17.E and 42.A-42.E, respectively). EVVVKLF (light grey) forms hydrogen bonds (yellow lines) with the chain-A 17LVFFA21 (dark grey), right after molecular docking and energy minimization. More bonds are formed by the end of the simulation. (B) RMSF per residue plot, after 600 ns of molecular dynamics simulations. (C) RMSD over time plot. (D) The total

number of residues in β-sheets, according to DSSP, over time. (E) Number of intermolecular hydrogens bonds, between Aβ42 and EVVVKLF, over time.

Figure 6

Predicted natively disordered regions, aggregation-prone regions, and putative amphipathic α-helices on human clusterin α-chain. All aggregation-prone regions are located near the predicted natively disordered regions. 12NFHAMFQ18 is located on a putative amphipathic α-helix, while 177EVVVKLF183 is partly predicted as natively disordered.

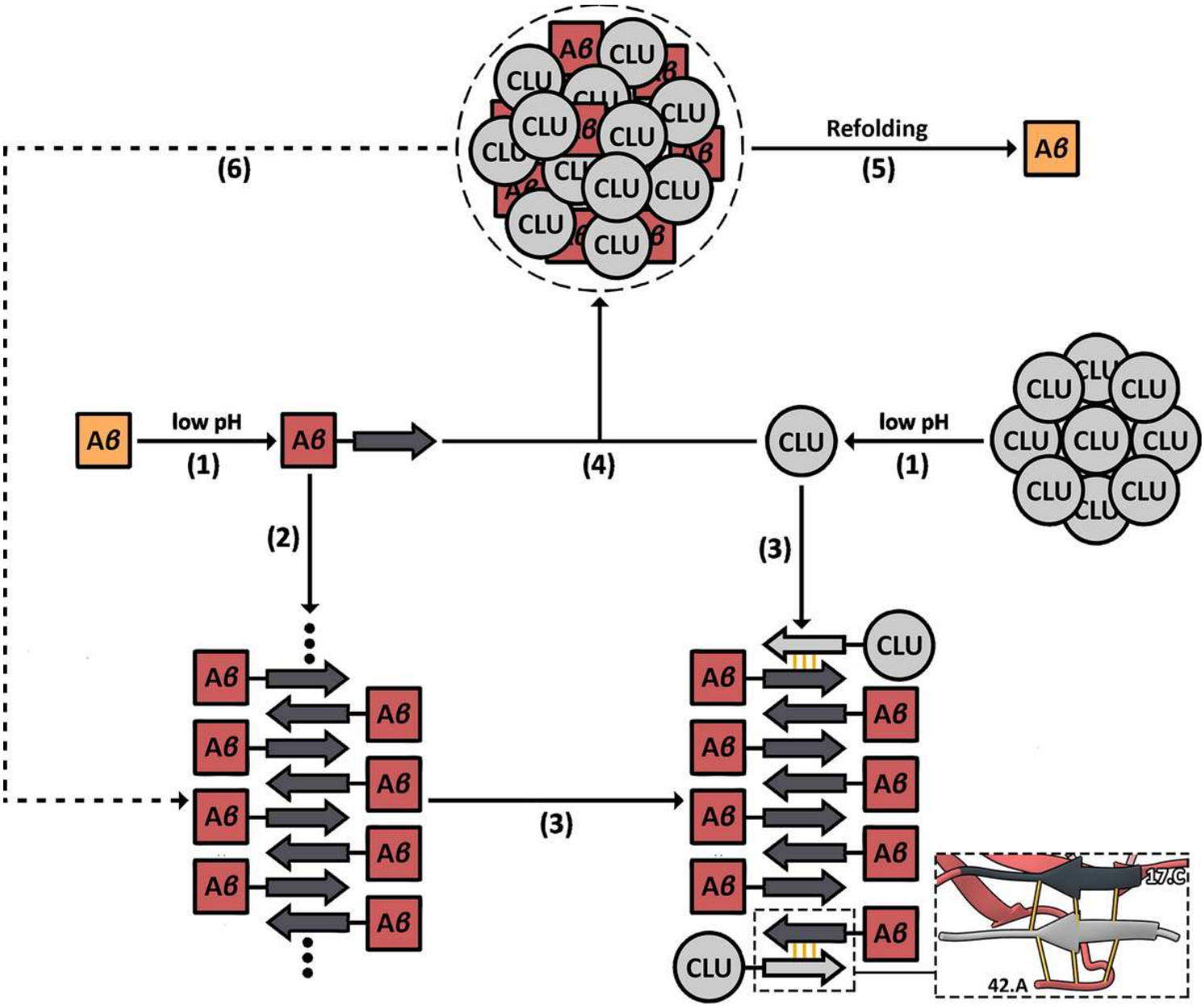

Figure 7

Putative mechanism of clusterin-mediated inhibition of Aβ amyloidogenesis. (1) Under acidic pH-induced stress, Aβ may partially unfold, exposing hydrophobic regions with the propensity to form β-strands. At the same time, the acidic pH triggers the disassociation of clusterin's heterogeneous aggregates. (2) Misfolded Aβ begin to form amyloid fibrils, but (3) the disassociated clusterin subunits (CLU) halt fibril growth, utilizing their aggregation-prone regions, which tend to form β-strands as well. The outlined picture is derived from the last frame of the molecular dynamics simulation of Aβ42+EVVVKLF. (4) Clusterin binds misfolded Aβ monomers, forming complexes and stabilizes their structure, until (5) they are refolded by other molecular chaperones. (6) In case misfolded Aβ species are produced faster than clusterin can stabilize their structure, it essentially brings them into proximity with remote monomers, accelerating amyloid formation.

Supplementary Files

This is a list of supplementary files associated with this preprint. Click to download.

- figures1.png
- figures2.png